^{210}Pb-based dating of recent sediments with χ-mapping versions of the CFCS, CIC, CF and TERESA models

J.M. Abril-Hernández

Departamento de Física Aplicada I, Universidad de Sevilla, Spain

A B S T R A C T

The ^{210}Pb-based method allows for absolute age determination in recent sediments on the centennial scale. The most common sedimentary scenarios involve ideal deposition without any further redistribution. The conventional models apply to such conditions by adding specific assumptions that allow analytical formulations: constant flux (CF), constant initial concentration (CIC), and constant flux with constant sedimentation (CFCS). The χ-mapping models are presented as a novel methodological approach. They generate a large number (10^5 to 10^6) of potential solvers, consisting of sets of n (the number of slices in the core) values of initial activity concentrations, A_0, and sedimentation rates, w. Empirical data serve to attract the solver that minimizes a χ function after encountering the best sorting along the core of the A_0 and w values. The specific assumptions of the above models are reformulated in terms of the statistical distributions of A_0 and w. The performance of the χ-mapping versions is demonstrated with a set of cores from the literature with independent chronologies. The main advantages compared to known analytical formulations are: i) χ-mapping provides a more robust fitting method. ii) It overcomes the problem of age reversals often found in the CIC model. iii) The CF model successfully applies to cores with unsteady and/or incomplete inventories. iv) The TERESA model (time estimates from random entries of sediments and activities), without analytical counterpart, is the only model that can manage continuous trends of change in the fluxes of unsupported ^{210}Pb. The work discusses the conditions for compensating model errors in the chronologies, and the use of the palaeorecords of fluxes, A_0 and w. The methodology can be extended to other assumptions (models) and provides novel and insightful views on the ^{210}Pb-based dating of recent sediments.

1. Introduction

The ^{210}Pb-based method allows for absolute age determination in recent sediments at centennial scale (Caroll and Lerche, 2003). The technique relays on the geochemical cycling of ^{210}Pb ($T_{1/2}$ = 22.3 a) in nature (Robbins, 1978), and distinguishes two fractions in the total ^{210}Pb content of a sediment sample: i) supported ^{210}Pb, assumed in secular equilibrium with its parent radionuclide ^{226}Ra, and ii) unsupported or excess ^{210}Pb, labelled hereafter as ^{210}Pb$_{exc}$. The latter is ultimately of atmospheric origin (from the decay of ^{222}Rn gas), but in aquatic environments it can be bound to solid particles at different stages on its path towards the final sedimentary deposits (Mabit et al., 2014).

Lead-210 is known to show a very high affinity for solids, so in most cases the approach of considering the accreting sediment as a continuous medium is justified. The advection-diffusion equation with radioactive decay then governs the spatial and temporal changes in the ^{210}Pb$_{exc}$ concentrations, with a bulk density governed by a compaction

potential and a conductivity function (Abril, 2003, 2011). It can be conveniently rewritten in terms of mass depth, m, avoiding the problem of unsteady bulk densities (Abril, 2003).

The above approach requires the continuity of the sedimentary sequence and discarding erosion and massive depositional events. Solving the equation requires a parameterisation of the spatial and temporal variability of the diffusion coefficient and providing initial and boundary conditions. The continuity of fluxes (of mass and of ^{210}Pb$_{exc}$) at the sediment-water interface (SWI) is the common adopted approach for these last, and the absence of diffusion and translocational mixing is a widespread sedimentary condition. The equations are deterministic, so the solution is unique for any stated settings. However, the reverse is not true, as demonstrated in Abril (2015). This implies that the empirical data set does not unambiguously define a chronology (an age-depth relationship). The chronology cannot be decoded without a series of assumptions on the prevailing sedimentary conditions (e.g., on the temporal variability of accretion rates and ^{210}Pb$_{exc}$ fluxes; and on the existence and parameterisation of diffusion). There are different

possibilities for selecting such assumptions. Each functional choice is referred to as a ^{210}Pb-based dating model; and different models potentially lead to different chronologies. A summary of these models can be seen, among others, in Mabit et al. (2014) or Arias-Ortiz et al. (2018), and an R software package is presented in Bruel and Sabatier (2020).

This work focusses on the most common sedimentary conditions that meet: i) continuity of the sedimentary sequence; ii) absence of post-depositional redistribution; iii) ideal deposition of fluxes of mass (sedimentation rates, SARs) and ^{210}Pb$_{exc}$ in the SWI over previously existing material.

After coring and sectioning the sediment into n slices, mass activity concentrations of ^{210}Pb and ^{226}Ra can be measured for each slice, and ^{210}Pb$_{exc}$ is routinely estimated as their difference on a layer-by-layer basis. A_k denotes the mass activity concentration of ^{210}Pb$_{exc}$ in the slice of index k ($k = 1, 2, …, n$), and Δm_k is its mass thickness ($\Delta m_k = \rho_{b,k} \Delta z_k$, with $\rho_{b,k}$ the bulk density of the slice, and Δz_k its depth thickness). Both magnitudes are known with their respective analytical uncertainties, $\sigma_{A,k}$ and $\sigma_{\Delta m,k}$.

A chronology, $T(m)$, gives the age of the horizon at mass depth m referred to the date of sampling (the SWI is of age zero). If such a chronology was available, as is the case for varved sediments, then it would be possible to estimate the palaeorecords of SARs, w_k, and initial activity concentrations of ^{210}Pb$_{exc}$, $A_{0,k}$ in the absence of post-depositional redistribution (see the sketch in Fig. 1 for clarifying the notation):

$$w_k = \Delta m_k / \Delta T_k \tag{1a}$$

$$A_{0,k} = A_k e^{\lambda T_{k-1}} \frac{\lambda \Delta T_k}{1 - e^{-\lambda \Delta T_k}} ; \tag{1b}$$

$$\Delta T_k = T_k - T_{k-1} ; \quad k = 1, …n \tag{1c}$$

w_k is the time-averaged value of the sedimentation rate in the time interval ΔT_k during which the mass thickness Δm_k of the slice k was deposited. Note that A_k is a physically averaged value (because homogenization of the sample), and $A_{0,k}$ is the equivalent constant value of ^{210}Pb$_{exc}$ concentration when the slice was accreted in the SWI (λ is the radioactive decay constant for ^{210}Pb). The continuity of the flux of ^{210}Pb$_{exc}$, F [Bq m^{-2}a^{-1}], at the SWI under the above assumptions allows estimating the equivalent constant flux during the formation of the slice of index k, as

$$F_k = A_{o,k} w_k \tag{2}$$

These palaeorecords of w_k and $A_{0,k}$ provides valuable information on the sedimentary conditions and their changes with time during the range
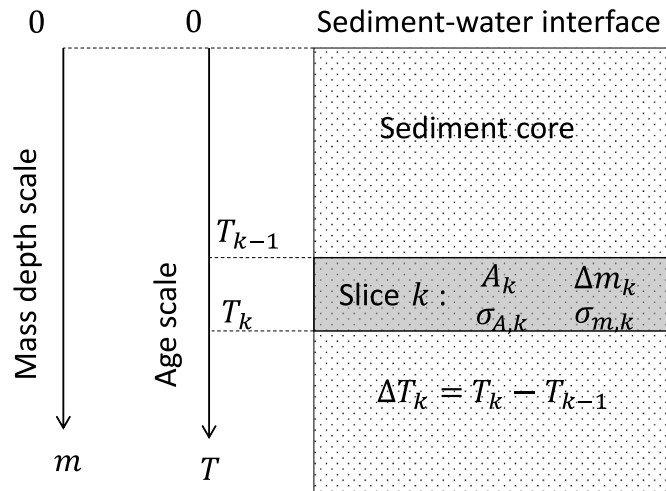
of the chronology (e.g., Abril and Brunskill, 2014; Abril, 2022).

However, ^{210}Pb-based dating pursues the reverse problem of extracting a chronology from the dataset ($A_k, \Delta m_k$), along with some complementary information about past sedimentary conditions. This is, the problem is to find a set of n ($A_{o,k}, w_k$) pairs so that Eq. (1) can be reverted to reencounter the empirical data set ($A_k, \Delta m_k$). Therefore, the time intervals could be solved as $\Delta T_k = \Delta m_k / w_k$, allowing the for the construction of the chronology $T_k = T_{k-1} + \Delta T_k$, and solving A_k from $A_{o,k}$ by reverting Eq. (1b).

As discussed previously, there are an infinite number of n ($A_{o,k}, w_k$) pairs being a mathematically exact solution of the above problem, involving different chronologies. The researcher must adopt some simplifying assumptions on the sedimentary conditions, such as fluxes and/or initial activity concentrations of ^{210}Pb$_{exc}$ being constant over time. Then, the problem can be faced by generating a large number ($\sim 10^5$) of different tentative n ($A_{o,k}, w_k$) pairs, now fulfilling the specific model assumption, so that the profiles A_k^* obtained by reverting Eq. (1) (denoted with *) can be compared with the empirical one by using function:

$$Q^2 = \sum_{k=1}^{n} \frac{\left(A_k^* - A_k\right)^2}{\sigma_{A,k}^2} \tag{3}$$

The $\chi^2 = Q^2 / f$ function involves the number of degrees of freedom, $f = n - p + 1$, with p being the number of free parameters in the model (Bevington and Robinson, 2003). The best solution for the problem will be the one that minimizes Q^2 (or χ).

This strategy is relatively easy to implement in computer codes with low CPU cost. The cloud of different tentative n ($A_{o,k}, w_k$) pairs, referred hereafter as *solvers*, can be systematically generated, so that χ^2 can be mapped to find the absolute minimum. In other words, the specific model assumptions serve to generate a cloud with a very large number of solvers, and the empirical dataset is used as the attractor for the best solution. This solution is expected to provide a reasonable proxy for the true (but generally unknown) chronology.

This was in essence the modelling strategy first used for the TERESA (Time Estimates from Random Entries of Sediments and Activities) model (Abril, 2016; Botwe et al., 2017). Here, such a strategy will be adapted to the assumptions of the most common dating models, developing their χ-mapping versions, namely the constant flux with constant sedimentation model (CFCS) (Robbins, 1978), the constant initial activity model (CIC) (Goldberg, 1963), and the constant flux model (CF), which contains as a particular case the constant rate of supply model (CRS) (Appleby and Oldfield, 1978). This will show new capabilities for these models and new methods for estimating uncertainties in the resulting chronology. The use of these χ-mapping versions of the models will be demonstrated through application to real cases from literature data with known independent chronologies.

Reference dates, such as the ^{137}Cs peaks linked to its known atmospheric deposition history, when available, can be used as external validation of the ^{210}Pb-based chronology (Smith, 2001), or alternatively, to formulate new attractors for the best solution (Abril, 2016).

There is a great deal of empirical evidence that the most common sedimentary conditions involve ^{210}Pb$_{exc}$ fluxes and SARs that largely vary over time and achieve a positive statistical correlation among them (Abril and Brunskill, 2014). It could be thought that, as this is in contradiction with their basic assumptions, the CFCS, CIC, and CF models should be of marginal use. However, it has been shown that the mathematical formulations of these models have some ability to compensate for positive and negative deviations of the chronology (Abril, 2019, 2020). This work will extend such studies to the χ-mapping versions of the models.

Fig. 1. Sketch illustrating the empirical measurements in a sediment slice.

2. Methods

2.1. Formulation of the specific model assumptions in terms of $(A_{o,k}, w_k)$

The $A_{o,k}$ values can be seen as a sample of size n of a certain statistical distribution (Abril and Brunskill, 2014). The specific limiting probability density function is a model assumption. The same applies to the n w_k values. The most simple and natural approach is to assume that the above sets of values are normally distributed around their arithmetic means, as inferred by Abril and Brunskill (2014) from a wide statistical study with varved sediments. However, other possibilities can be considered.

2.1.1. CFCS model

The model assumes that the n w_k takes the same value $\overline{w}$ (a constant sedimentation rate), and that the n $A_{o,k}$ take the same value $\overline{A}_o$ (constant initial concentration), so that the flux is constant (from Eq. (2)). From a mathematical view point, the model assumes that w_k and $A_{o,k}$ fit a Dirac's delta distribution. The model has two free parameters, namely $\overline{A}_o$ and $\overline{w}$, which will be the parametric lines of a χ function.

The well-known analytical solution of the CFCS model is the following:

$$A(m) = A_o e^{-\lambda \frac{m}{w}} \tag{4}$$

Eq. (4) allows determining A_o and w from a curve-fitting. In this model, these two magnitudes are coincident to $\overline{A}_o$ and $\overline{w}$. However, there are some practical considerations. First, Eq. (4) applies to a continuous medium, while the experimental data refer to a discrete slicing. The most popular fitting procedure is the linear fit of LN $[A_k(m)]$ using a least squares method that does not take into account the analytical uncertainties in A_k, nor the thickness of the mass depth intervals where they are defined. There are other fitting methods that lead to slightly different results, such as minimizing absolute deviations, using the medium of three groups, orthogonal regression, or calibration models weighted by $\sigma_{A,k}$. The χ-mapping version compares model and empirical values of the same nature (mean values in the Δm_k interval), weighted by $\sigma_{A,k}$, so it provides a more robust fitting method.

2.1.2. CF model

The χ-mapping version of the model assumes that the n $A_{o,k}$ values are normally distributed around their arithmetic mean $\overline{A}_o$, with a certain standard deviation σ_A. The relative deviation is $s_A = \sigma_A / \overline{A}_o$. Note that this is not in contradiction with their sorting along the core, which may result in patterns of increase, decrease, or any other.

The assumption of a constant flux implies that (from Eq. (2)): $w_k = \frac{F}{A_{o,k}}$. The definition of $w_C = F/\overline{A}_o$ will be of practical use.

The model uses three free parameters, namely $\overline{A}_o$, w_C and s_A, being the parametric lines of a χ function.

Note that this version of the CF model does not need a complete recovery of the total inventory, Σ_0, nor the assumption of its steady state, as required for the CRS model. Note that the classical formulation (Appleby and Oldfield, 1978) relates Σ_0 with the inventory below the horizon at mass depth m, Σ_m, with the age T_m of such horizon:

$$\Sigma_m = \Sigma_0 e^{-\lambda T_m} \tag{5}$$

In particular, the new χ-mapping formulation allows dating recent sediment cores that grow under a constant F (in practise, under varying F but with randomly distributed variability) but that have not yet reached a steady-state inventory, such as in the cases of sediments that grow in a reservoir after damming or in a harbour after dredging. In this χ-mapping version the alternative assumption of normally distributed $A_{o,i}$ values is used instead.

2.1.3. CIC model

The model assumes that the n $A_{o,k}$ take the same value $\overline{A}_o$ (constant initial concentration). For the n w_k values, in this particular χ-mapping version it will be assumed that they are normally distributed around their arithmetic mean value $\overline{w}$, with standard deviation σ_w, and a relative standard deviation $s_w = \sigma_w/\overline{w}$. This is a three-parameter model ($\overline{A}_o$, $\overline{w}$ and s_w).

Note that this χ-mapping version includes the soft extra assumption of normally distributed w_i values, which is not necessary for the classical analytical formulation of the CIC model:

$$A(m) = A_o e^{-\lambda t} \tag{6}$$

The problem of age reversals is known with this model in cores where the $A(m)$ profile is not smooth enough. The present version overcomes this problem, as will be shown in the application cases. However, this model produces poorer fits. The reason is clear from the reverted Eq. (1) and after a second-order expansion:

$$A_k = A_{o,k} \frac{1 - e^{-\lambda \Delta m_k / w_k}}{\lambda \Delta m_k / w_k} e^{-\lambda T_{k-1}} \cong A_{o,k} e^{-\lambda T_{k-1}} \left(1 - \frac{\lambda}{2} \frac{\Delta m_k}{w_k} \right) \tag{7}$$

Thus, a change by a factor two in $A_{o,k}$ automatically translates into a change of equal size in A_k, while such a change in w_k yields changes of the order of 2%–5%. Consequently, those models that do not allow variability in A_0 have poor performance in cores with irregular $A(m)$ profiles.

2.1.4. TERESA model

The model allows for simultaneous and independent variability in A_0 and SARs, with the only assumption (in its basic version) of that both follow normal distributions around their respective arithmetic mean values. This is a four-parameter model ($\overline{A}_o$, $\overline{w}$, s_A and s_w). Full details on this model can be found in Abril (2016, 2022).

2.1.4.1. Models with non-normal distributions.
The use of log-normal distributions with the TERESA model was explored by Abril (2016). Multimodal distributions can be used with TERESA in complex sediment cores, as shown by Abril (2020). In sediments affected by anthropogenic sources of ^{210}Pb bound to particles, such as phosphogypsum generated in the phosphate industry, mixed with materials of natural origin, initial activity concentrations and sedimentation rates may be interdependent. These cases will not be treated here, but are mentioned to highlight that the χ-mapping strategy could potentially be adapted to face these problems.

2.2. Numerical solution

For the numerical solution of the above models, it is necessary to generate a cloud of solvers over a regular mesh in the parametric space. For each solver, a sorting algorithm decides the best arrangement downcore of the pairs, and its global performance is quantified through the χ-function. The model solution is given by the absolute minimum of χ. The details to solve the TERESA model can be found in Abril (2016), and the numerical codes are available for scientific evaluation as supplementary material in Abril (2020). The required adaptations for the χ-mapping versions of the CFCS, CIC, and CF models are relatively easy to implement. Details are presented in Annex A, in electronic supplementary material (ESM). For the present work, a set of codes has been written in the BASIC language using Quick-Basic software and run under an MSDOS emulator.

2.3. Application to real cores

Core C1 is a varved sediment sampled in April 1999 in the Pettaquamscutt River basin (Rhode Island, Northeast USA), 41°30′N, 71°26′W, at 19.5 m depth (data from Lima et al., 2005). The

reconstructed palaeorecords of *F*, *w* and A_o were presented in Abril (2020). This is a case with a relatively smooth profile of $A(m)$, with varying fluxes, but with such variability being randomly distributed along the time line (but at the bottom of the core). Thus, the CFCS, CRS, CIC, and TERESA models have a reasonable good performance, as shown with their analytical formulations in Abril (2020).

Core C2 is a varved sediment sampled in April 2011 in Lake Kevojärvi, Finland (69°45′N, 27°00′ E) at 35 m water depth (data from Haltia et al., 2021). Details on the treatment of raw data can be seen in Abril (2023b).

Core C3 was sampled in February 1988 at Senhouse Dock, Maryport, UK (data from Kershaw et al., 1990). It is a 2 m long composite core, with high resolution slicing. A detailed study of this core has been presented elsewhere (Abril, 2023a).

Core C4 is a varved sediment core sampled in 1971 in the Santa Barbara Basin (data from Koide et al., 1973). The reconstructed palae-orecords of *F*, *w* and A_o were presented in Abril (2020). In this case, the fluxes show a continuous increase trend in recent times.

3. Results and discussion

3.1. Testing the performance of the models with core C1

3.1.1. CFCS model

Fig. 2 shows the empirical $^{210}Pb_{exc}$ versus mass depth profile for core C1 along with the best fit obtained with the χ-mapping version of the CFCS model. It has been obtained after a few iterations with meshes of 10^4 pixels in the $[\overline{A}_0, \overline{w}]$ plane. Each iteration gives a χ-surface for which the absolute minimum is found after comparing the 10^4 values. The subsequent iterations increased the resolution of the mesh around the absolute minimum. It is compared against the analytical solution of Eq. (4) with parameters solved by two different fitting methods using Stat-graphics Centurion 18. The corresponding chronologies are depicted on the secondary Y-axis and compared with the varve chronology.

The estimation of uncertainties in the fitting parameters for the χ-mapping model is illustrated in Fig. 3. For the other fits, errors have been estimated with the Satgraphics Centuriun software. They are reported in Table 1. The χ-mapping version of the model provides the best fit (the lowest χ value), with smaller uncertainties in the fitting parameters, and with a very close match to the varve chronology.
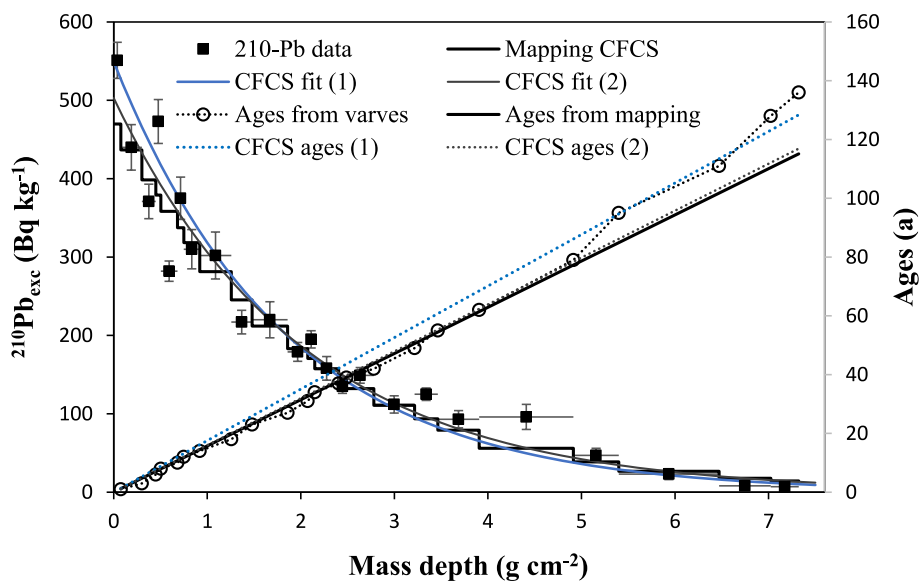

Fig. 3. Parametric lines around the absolute minimum of the Q^2 function (Eq. (3)), along with polynomial fits, which served to estimate the uncertainties in parameters (see Annex A, in ESM), as reported in Table 1.

Table 1
Fitting parameters for the CFCS model using different numerical methods (Core C1).

Method	A_o			*w*			χ
Linear least squares fit	549	±	48	0.057	±	0.003	2.68
Orthogonal regresion	569	±	51	0.056	±	0.003	2.89
Calibration method using $\sigma_{A,k}$ weights	503	±	32	0.063	±	0.003	2.37
χ-mapping	478.5	±	7.5	0.064	±	0.001	2.30

Fig. 2. $^{210}Pb_{exc}$ versus mass depth for core C1. Vertical bars are 1-σ analytical uncertainties, while horizontal bars define the mass-depth interval of the slices. The stepped line is the best fit with the χ-mapping version of the CFCS model. The analytical solution of Eq. (4) after a least-squares linear fit and a weighted fit are fit (1) and fit (2), respectively. The ages from the varves and from the models are depicted on the secondary Y-axis (error bars are omitted for the sake of clarity).
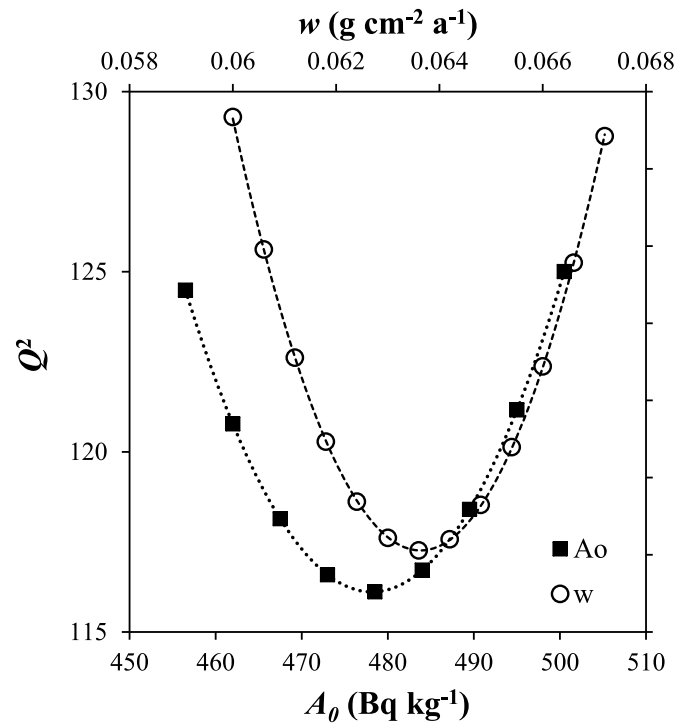
Deviations of the model profiles from the empirical one are quite apparent in Fig. 2, and they are attributable to model errors (deviations are due to the partial achievement of the assumption of constant flux and constant sedimentation rate). However, these model errors result in positive and negative deviations in the model chronology that tend to mutually compensate downcore (Fig. 2).

3.1.2. CIC model

Fig. 4 shows the result of the application of the χ-mapping version of the CIC model to core C1. The model parameters for the best fit and their associated uncertainties (Annex A, ESM) were: $\overline{A}_0 = 506.5 \pm 3.5$ Bq kg^{-1}, $\overline{w} = 0.0639 \pm 0.0004$ g cm^{-2} a^{-1}, and $s_w = 0.212 \pm 0.004$, with $\chi = 2.09$. This results in a chronology that closely matches the one from varves (but for older layers). The 1-σ propagated uncertainties were below 1.5%, accounting the model errors for larger deviations from the varve chronology. It is worth noting that the extra assumption of normally distributed sedimentation rates and the use of Eq. (1) prevent the larger deviations and age reversals that usually appear with the application of the analytical formulation of the CIC model (Eq. (6) and Fig. 4).

3.1.3. CF model

Fig. 5 shows the application of the χ-mapping version of the CF model to core C1. The model parameters for the best fit and their associated uncertainties were: $\overline{A}_0 = 485.0 \pm 1.6$ Bq kg^{-1}, $w_C = 0.0650 \pm 0.0002$ g cm^{-2} a^{-1}, and $s_A = 0.189 \pm 0.011$, with $\chi = 0.45$. This results in a chronology that is in close agreement with that of varves, with1-σ propagated uncertainties below 1.5%. The chronology from the CRS model (Eq. (5)) is depicted for the sake of comparison. The missing part of the total inventory has been estimated by the reference SAR method (Appleby, 1998). The correction is only 0.9%, but it strongly affects older ages, which would have been larger without such a correction.

3.1.4. TERESA model

This model does not have an analytical version to compare with. Fig. 6 shows five runs of the model using different random arrangement of the (z_i, z_j) pairs (see Annex A, ESM). The χ value for the best fit of each run ranged from 0.31 to 0.44, and the cloud of chronological lines agrees fairly well with the ages from the varves. Deviations are attributable to

model errors, which in this case arise from the assumption of normally-distributed A_o and w values, and the use of the canonical sample of size n.

As an example, for run *R1*, the fitting parameters were $\overline{A}_0 = 505.0 \pm 1.2$ Bq kg^{-1}, $\overline{w} = 0.0624 \pm 0.0010$ g cm^{-2} a^{-1}, $s_A = 0.200 \pm 0.006$, and $s_w = 0.112 \pm 0.001$, with $\chi = 0.44$.

3.1.5. Palaeorecords of A_o and w from the models

Despite the different involved assumptions, the four models show the ability of compensating positive and negative deviations in the chronology, so that model ages are a good proxy to the true ages (from varves). Noisy deviations in the chronology result in spurious values of the SARs, as shown by Abril (2022). However, as also shown in this reference, A_o are less sensitive to model errors, so their paleo-records generated by the models are useful for tracking past changes in sedimentary conditions. The CF and TERESA models explicitly solve the temporal records of A_o, while the CIC and CFCS models assume a constant value. However, for all models, the resulting chronology can be used to infer the palaeorecords of A_o and w by using Eq. (1). This is illustrated in Fig. 7.

The temporal variability in A_o, as inferred from varves, is randomly distributed along the time line, but in the deeper part of the core, where it exhibits a trend of increase. A more detailed study of this core in terms of piecewise versions of the models (in their classical formulations) has been presented elsewhere (Abril, 2020).

All the studied models are able to closely track the temporal variability of A_o in this core, as shown in Fig. 7. For TERESA and CF, the models already output the palaeorecords of A_o and w. The latter are coincident with the records estimated from Eq. (1) using the output chronology, while for the former, values from both methods slightly differ (Fig. 7). The four χ-mapping models are able to capture the mean value of SAR, but with spurious variability that does not match the palaeorecords estimated from the varve chronology.

3.2. Testing the performance of the models with core C2

Fig. 8 summarises the application of the χ-mapping versions of the models CF, CIC, and TERESA to core C2 (Lake Kevojärvi, data from Haltia et al., 2021). The fitting parameters are presented in Table 2. Only
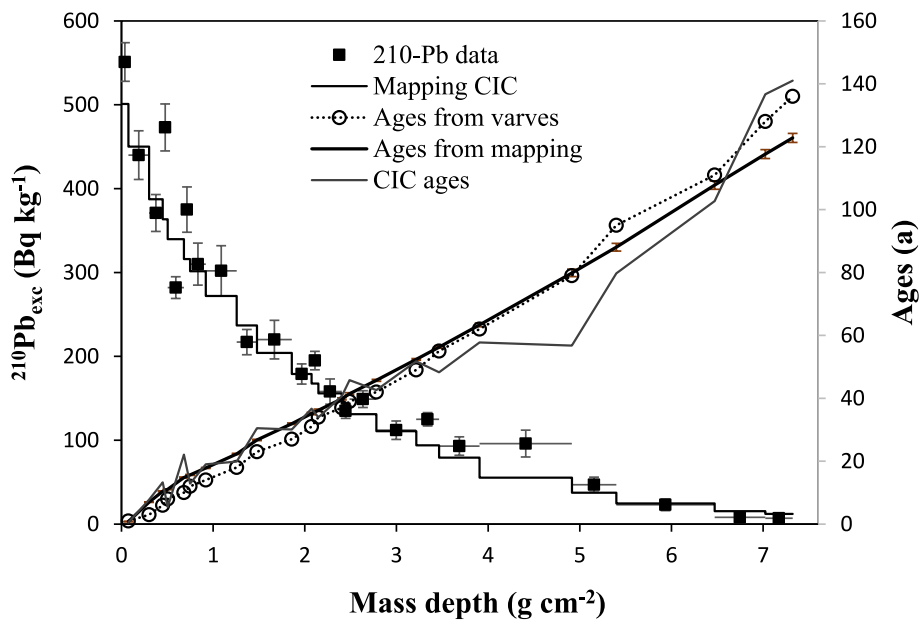
Fig. 4. $^{210}Pb_{exc}$ versus mass depth for core C1, as in Fig. 2. The stepped line is the best fit with the χ-mapping version of the CIC model. The ages of the varves and the model are depicted in the secondary Y-axis (error bars are 1-σ propagated uncertainties). The chronology from the analytical formulation of the CIC model (Eq. (6), with $A_0 = 560$ Bq kg^{-1}) is depicted for the sake of comparison.
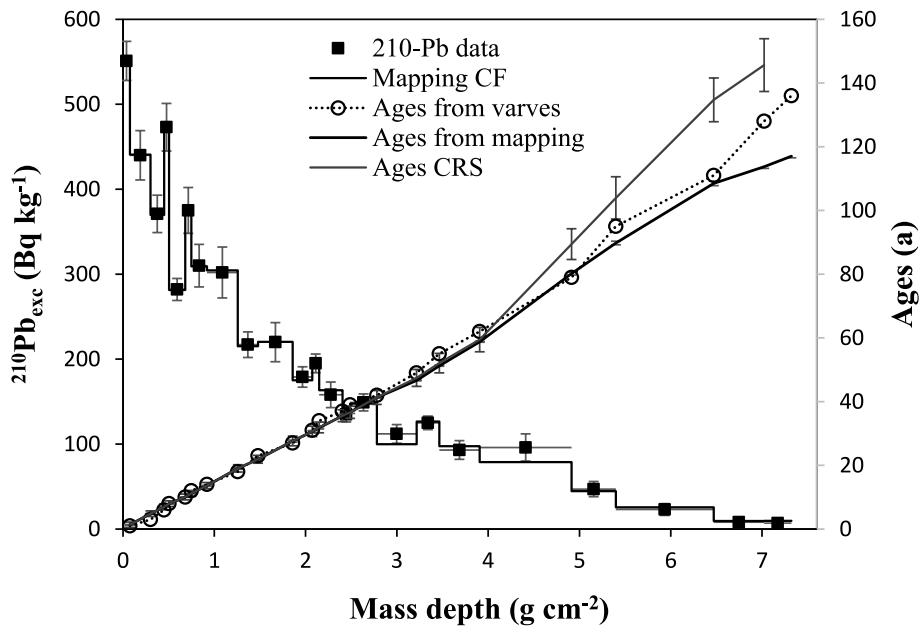
Fig. 5. $^{210}Pb_{exc}$ versus mass depth for core C1, as in Fig. 2. The stepped line is the best fit with the χ-mapping version of the CF model. The ages of the varves and the model are depicted in the secondary Y-axis (error bars are 1-σ propagated uncertainties). The chronology from the analytical formulation of the CRS model (Eq. (5)) is depicted for the sake of comparison.

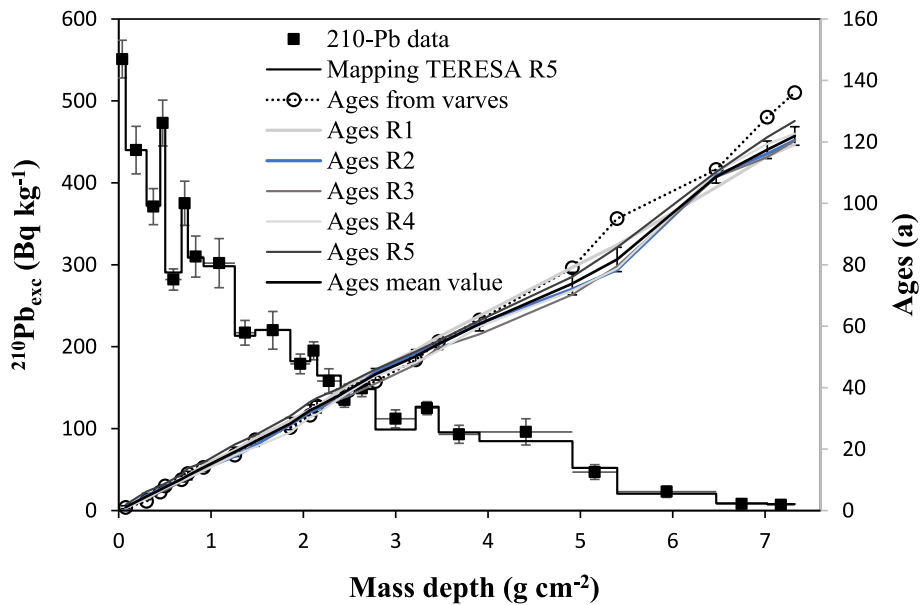**Fig. 6.** $^{210}Pb_{exc}$ versus mass depth for core C1, as in Fig. 2. The stepped line is the best fit with the TERESA model. The ages from the varves and from five runs of the model are depicted on the secondary Y axis. Each run corresponds to a different random arrangement of the (z_i, z_j) pairs. The mean value of the model ages is depicted with the standard deviation (vertical bars).

one arrangement of the (z_i, z_j) pairs was used for this application of the TERESA model.

The CF and TERESA models accurately fit the empirical $A(m)$ profile, producing chronologies in reasonably good agreement with that from varves. The CIC model only allows variability in SARs, which are less influencing than A_o for adapting to the irregularities in the empirical profile, so that only a smooth trend line is captured. However, the model chronology still compares with that from varves, and without age-reversals issues.

Fig. 9 shows the initial activity concentrations and SARs estimated from the varves for the core C2. The former are normally distributed around the arithmetic mean value, with $p = 0.542$ after a Kolmogorov-

Smirnov test. The distribution of SARs is compatible with a normal distribution, but with $p = 0.084$ from the above test. The fluxes (from Eq. (2)) linearly correlated with SAR with $p < 0.001$. As in the case of core C1, the direct outputs of the CF and TERESA models closely fit the largely varying A_o values from varves, while they only capture the mean values of SARs. Note that the temporal variability of A_o and w is randomly distributed along the time line. This condition is necessary for the good performance of the CF model, as shown for the analytical formulation of the CRS model in Abril (2019, 2020).
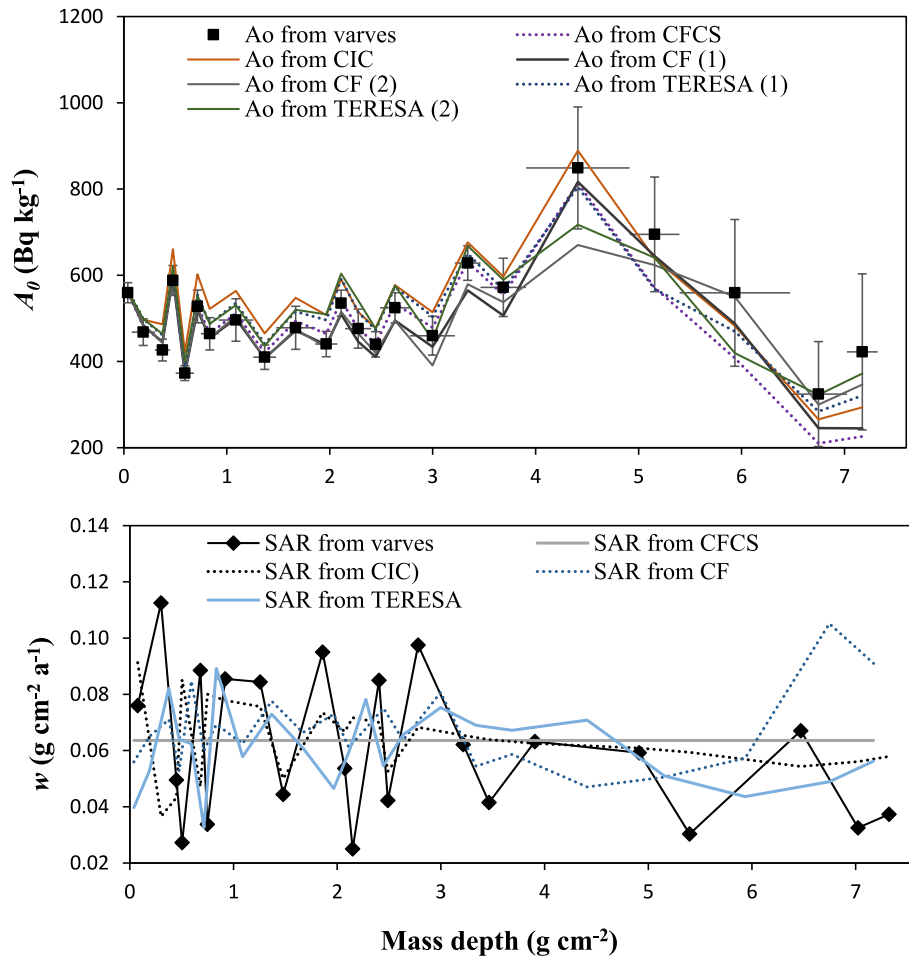
Fig. 7. Initial activity concentrations and SARs estimated by Eq. (1) from varves and the chronologies by the χ-mapping CFCS, CIC, CF, and TERESA models for core C1. For the last two, initial activity concentrations from direct model output are also plotted with label (2).
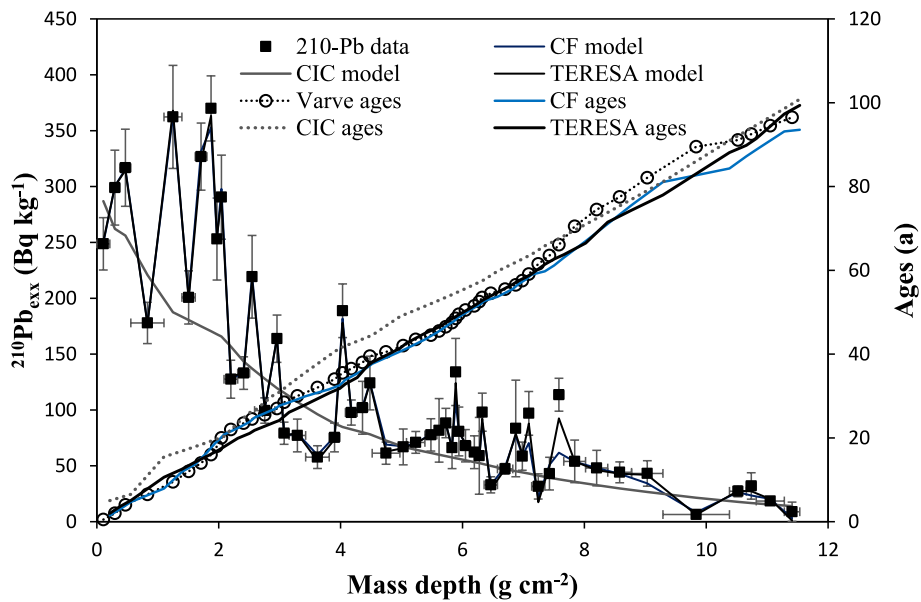

Fig. 8. $^{210}Pb_{exc}$ versus mass depth for core C2. Vertical bars are 1-σ analytical uncertainties, while horizontal bars delimit the thickness of the slices. The continuous lines are the best fits obtained with the χ-mapping versions of the CF, CIC and TERESA models (here the lines are connecting the model values, adscribed to the centre of each slice). The ages from the varves and from the three models are depicted in the secondary Y-axis (errorbars are omitted for the sake of simplicity).

Table 2

Model parameters for the application of the χ-mapping models to core C2.

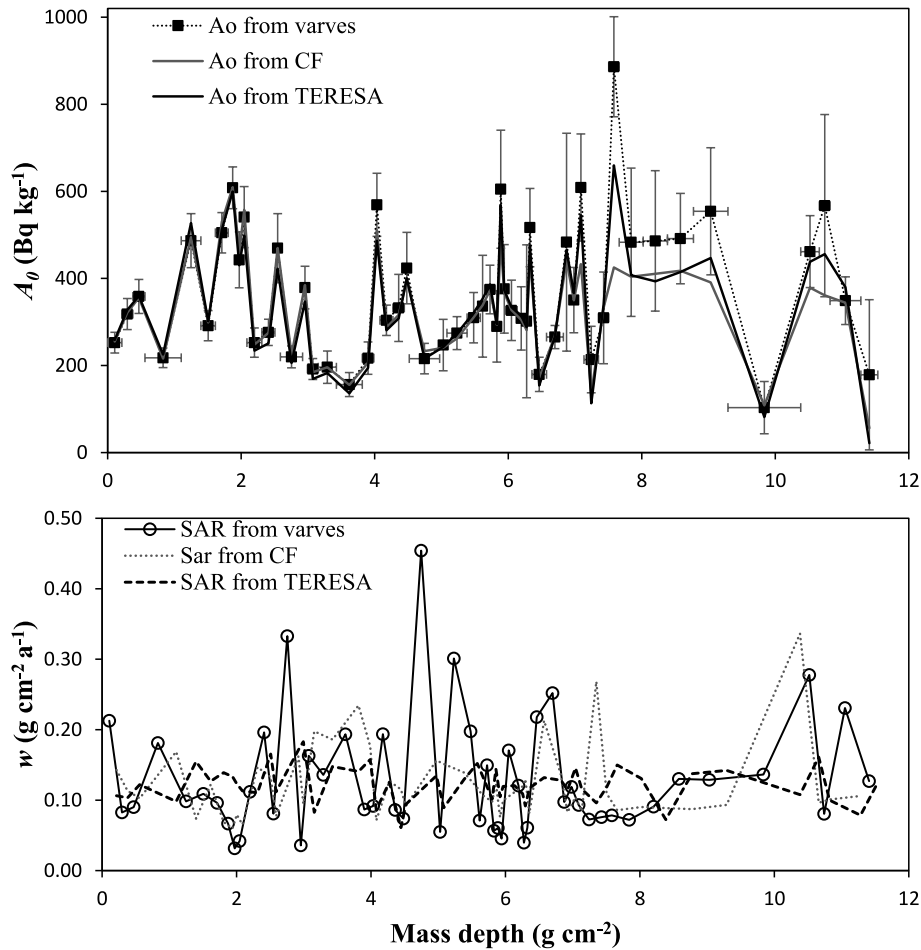| Model	$\overline{A}_o$ (Bq kg^{-1})			$\overline{w}$ or w_C (g cm^{-2}a^{-1})			s_A			s_w			χ
CF	333.0	±	0.6	0.1095	±	0.0013	0.360	±	0.003	- -			0.63
CIC	310	±	4	0.1414	±	0.0018	- -			0.299	±	0.005	2.39
TERESA	340.6	±	0.2	0.1219	±	0.0002	0.399	±	0.001	0.213	±	0.001	0.36

Fig. 9. Initial activity concentrations and SARs estimated from varves (Eq. (1)) and for direct outputs of the CF and TERESA models for core C2.

3.3. Performance of the CF and TERESA models with core C3

For core C3 (Maryport, UK; data from Kershaw et al., 1990) the authors presented an age-depth model for the 0–140 cm of the core based on the comparison of radionuclide profiles in the core with their decay-corrected Sellafield discharges. It will serve to test the performance of the models.

The empirical $A(m)$ profile is shown in Fig. 10. In the deepest sections of the core, $^{210}Pb_{exc}$ is above 40 Bq kg^{-1}, indicating that the core did not reach the level of dredging in the early 1950s. The retrieved inventory of $^{210}Pb_{exc}$ was 118.9 ± 1.1 kBq m^{-2}, a value approximately two orders of magnitude higher than expected from the atmospheric flux in the area (Kershaw et al., 1990). The application of the CRS model was not possible since the inventory was only partially recovered and because it was not in a steady state.

The χ-mapping version of the CF model does not require the total inventory, but the application of Eq. (1) requires continuous measurements. In this core, the raw data included few unmeasured slices for which linear interpolations were applied. The CF model was able to accurately fit the empirical profile ($\chi = 0.84$), producing a chronology in

reasonable agreement with the reference chronology of Kershaw et al. (1990) and with the results of the TERESA model (applied here with a single arrangement of the (z_i, z_j) pairs). The results are summarised in Fig. 10, and the fitting parameters are listed in Table 3.

Fig. 11 shows the palaeorecords of initial activity concentrations and fluxes, as estimated by the TERESA and CF models. For this last, the constant flux of 5550 ± 30 Bq m^{-2}a^{-1} captures the mean value of the highly varying fluxes estimated by the TERESA model, and that includes a stepped decrease in the mean value of the fluxes in the upper (younger) region of the core. In this region, the CF chronology deviates from the reference ages since the assumption of constant flux is strongly stressed. However, such deviations are progressively compensated for and the CF chronology converges towards the reference ages and the chronology from the TERESA model. It is worth noting the ability of the CF model to compensate for not only random variability in fluxes along the time line but also partially among transects with stepped changes in the mean values of fluxes.
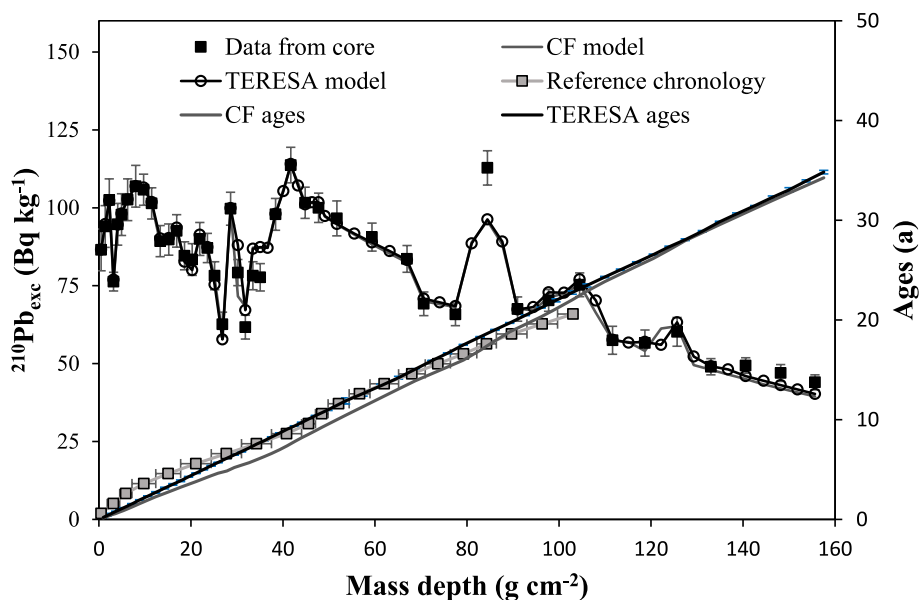
Fig. 10. $^{210}Pb_{exc}$ versus mass depth for core C3. Vertical bars are 1-σ analytical uncertainties. Continuous lines are the best fits obtained with the χ-mapping versions of the CF and TERESA models (the lines connect the model values, adscribed to the centre of each slice). The reference chronology and the ages of the models are depicted in the secondary Y axis (horizontal bars refer to the thickness of the slices).

Table 3
Model parameters for the application of the χ-mapping models to core C3.

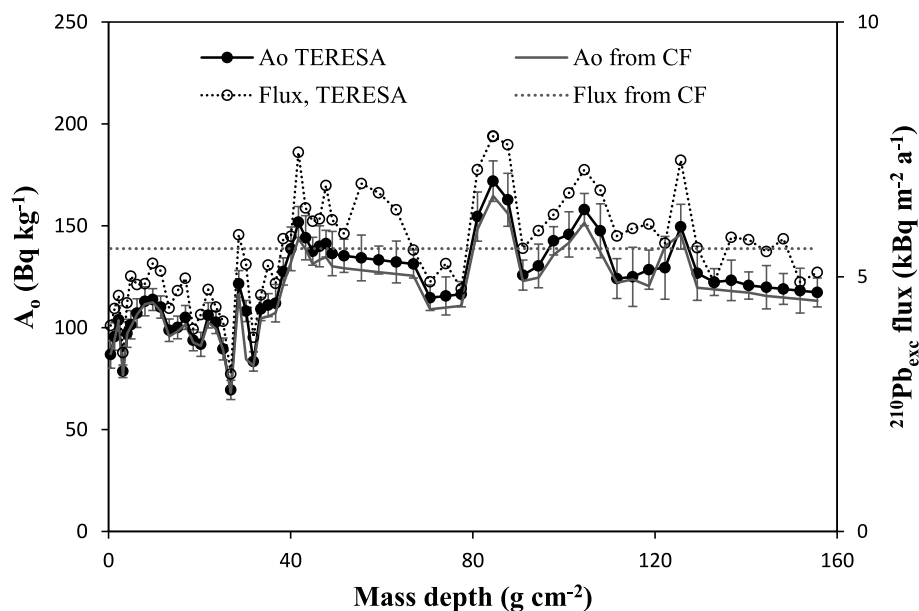| Model	$\overline{A}_o$ (Bq kg^{-1})			$\overline{w}$ or w_C (g cm^{-2}a^{-1})			s_A			s_w			χ
CF	116.4	±	0.2	4.770	±	0.024	0.172	±	0.002	- -			0.84
TERESA	120.7	±	0.2	4.540	±	0.002	0.176	±	0.001	0.050	±	0.002	0.80

Fig. 11. Palaorecords of the initial activity concentrations and fluxes estimated by the TERESA and CF models for the core C3.

3.4. Performance of the CF and TERESA models with core C4

The core C4 served to demonstrate the performance of the TERESA model and the failure of the CFCS and CRS models, under their analytical formulations (Abril, 2016). The reason for such a failure is a continuous trend of increase in fluxes in recent times, as demonstrated in Abril (2019). The aim here is to test the performance of the χ-mapping version of the CF model in this core. The results are summarised in Fig. 12 and Table 4. Both mapping models are producing virtually identical fits to the empirical $A(m)$ profile. However, the CF chronology systematically departs from that of varves (Fig. 12), in a similar way to that previously observed for the CRS model (Abril, 2019). The TERESA model, applied with a single arrangement of the (z_i, z_j) pairs, yields a chronology in reasonable agreement with that of the varves.
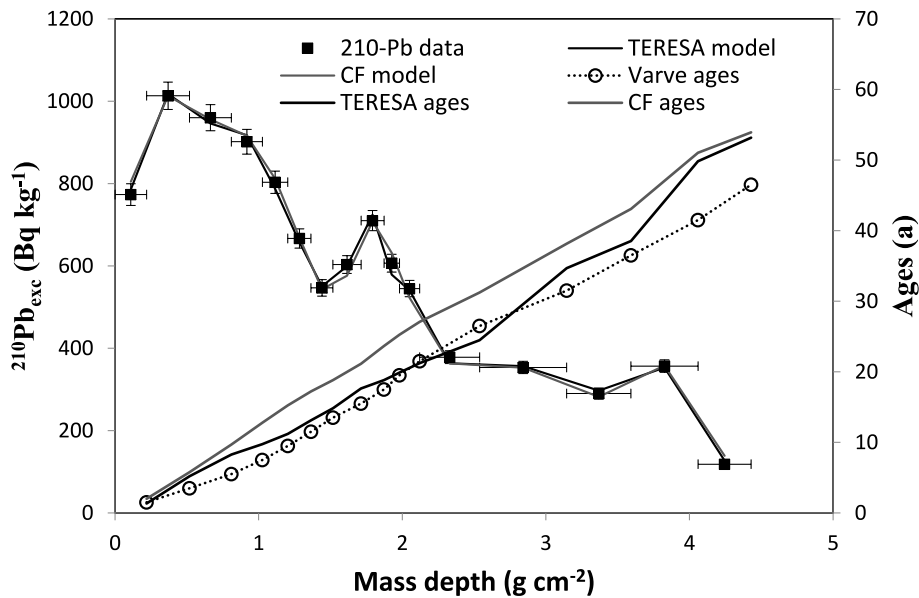
Fig. 12. $^{210}Pb_{exc}$ versus mass depth for core C4. Vertical bars are 1-σ analytical uncertainties, and horizontal bars define the thickness of the slices. The continuous lines are the best fits obtained with the χ-mapping versions of the CF and TERESA models (the lines are connecting the model values, adscribed to the centre of each slice). The chronology from the varves and the ages from the models are depicted on the secondary Y-axis.

Table 4
Model parameters for the application of the χ-mapping models to core C4.

Model	$\bar{A}_o$ (Bq kg^{-1})			$\bar{w}$ or w_C (g cm^{-2}a^{-1})			s_A			s_w			χ
CF	1125	±	2	0.0805	±	0.0002	0.1992	±	0.0004	- -			0.91
TERESA	1008	±	1	0.1029	±	0.0008	0.202	±	0.002	0.321	±	0.002	0.64

4. Conclusions

The main conclusions of this study were:

The χ-mapping versions have been presented for the models CFCS, CIC, CF and TERESA, and evaluated with a set of four real sediment cores with independent chronologies.

The χ-mapping CFCS model provides a more robust and accurate fitting method than those commonly used with its analytical formulation.

The χ-mapping CIC model assumes a constant A_0, with w values normally distributed. This overcomes the well-known problem of age reversals often found with the analytical version of the model.

The χ-mapping CF model assumes a constant value of F, with A_o values normally distributed. This avoids the need to assume a steady-state total inventory for the CRS model, as shown in core C3 with an incomplete and unsteady inventory.

The TERESA model does not have an analytical counterpart. It assumes, in its basic formulation, normal distributions for A_0 and w, being statistically independent. This means that their values can be randomly grouped. It has shown good performance in the four cores.

The performance of the models does not relay on the reliability of their assumptions, but on the capability of their mathematical architecture for translating model errors into positive and negative deviations in the chronology, so that they mutually compensate.

All models lead to reliable chronologies when the temporal variability in $^{210}Pb_{exc}$ fluxes (inferred from the varve chronology) is randomly distributed along the time line. These chronologies serve to reconstruct accurate palaeorecords of initial activity concentrations in all the cases.

Variability in A_0 and w differently affects to the output $A^*(m)$ profile. This explains the poor performance of the CIC model. By symmetry, the model SARs are largely affected by model errors, which prevents their use for tracking past changes in sedimentary conditions.

The χ-mapping version of the CF model fails in cases where the fluxes of $^{210}Pb_{exc}$ show a continuous trend of increase or decrease. This is in agreement with previous studies based on analytical formulations of the CRS and CFCS models.

TERESA is the only model that can face problems involving continuous trends of change in fluxes.

Declaration of competing interest

The authors declare that they have no known competing financial interests or personal relationships that could have appeared to influence the work reported in this paper.

Data availability

Data will be made available on request.

Appendix A. Supplementary data

Supplementary data to this article can be found online at https://doi.org/10.1016/j.quageo.2023.101484.

References

Abril, J.M., 2003. A new theoretical treatment of compaction and the advective-diffusive processes in sediments. A reviewed basis for radiometric dating models. J. Paleolimnol. 30, 363–370. https://doi.org/10.1023/B:JOPL.0000007220.16908.d4.

Abril, J.M., 2011. Could bulk density profiles provide information about recent sedimentation rates? J. Paleolimnol. 46, 173–186. https://doi.org/10.1007/s10933-011-9520-2.

Abril, J.M., 2015. Why would we use the Sediment Isotope Tomography (SIT) model to establish a ^{210}Pb-based chronology in recent-sediment cores? J. Environ. Radioact. 143, 40–46. https://doi.org/10.1016/j.jenvrad.2015.02.008.

Abril, J.M., 2016. A ^{210}Pb-based chronological model for recent sediments with random entries of mass and activities: model development. J. Environ. Radioact. 151, 64–74. https://doi.org/10.1016/j.jenvrad.2015.09.018.

Abril, J.M., 2019. Radiometric dating of recent sediments: on the performance of ^{210}Pb-based CRS chronologies under varying rates of supply. Quat. Geochronol. 51, 1–14. https://doi.org/10.1016/j.quageo.2018.12.003.

Abril, J.M., 2020. Multimodal-TERESA, a ^{210}Pb-based radiometric dating model for recent sediments under largely varying rates of supply. Quat. Geochronol. 55, 101032 https://doi.org/10.1016/j.quageo.2019.101032.

Abril, J.M., 2022. On the use of ^{210}Pb-based records of sedimentation rates and activity concentrations for tracking past environmental changes. J. Environ. Radioact. 244–245, 106823 https://doi.org/10.1016/j.jenvrad.2022.106823.

Abril, J.M., 2023a. Assessment of the performance of the ^{210}Pb-based dating models CFCS, CRS, and TERESA with a challenging sediment history. Quat. Geochronol. QUAGEO-D-23-00011R1 (under Review).

Abril, J.M., 2023b. ^{210}Pb-based dating of recent sediments with the χ-mapping version of the constant sediment accumulation rate (CSAR) model. J. Environ. Radioact. 268–269, 107247 https://doi.org/10.1016/j.jenvrad.2023.107247.

Abril, J.M., Brunskill, G.J., 2014. Evidence that excess ^{210}Pb flux varies with sediment accumulation rate and implications for dating recent sediments. J. Paleolimnol. 52, 121–137. https://doi.org/10.1007/s10933-014-9782-6.

Appleby, P.G., 1998. Dating recent sediments by [210]Pb: problems and solutions. In: Illus, E. (Ed.), Dating of Sediments and Determination of Sedimentation Rate. STUK A-145, Finland, pp. 7–24.

Appleby, P.G., Oldfield, F., 1978. The calculation of lead-210 dates assuming a constant rate of supply of unsupported ^{210}Pb to the sediment. Catena 5, 1–8.

Arias-Ortiz, A., Masqué, P., Garcia-Orellana, J., Serrano, O., Mazarrasa, I., Marbà, N., Lovelock, C.E., Lavery, P.S., Duarte, C.M., 2018. Reviews and syntheses: ^{210}Pb-derived sediment and carbon accumulation rates in vegetated coastal ecosystems: setting the record straight. Biogeosci. Discuss. https://doi.org/10.5194/bg-2018-78.

Bevington, P.A., Robinson, D.K., 2003. Data Reduction and Error Analysis for the Physical Sciences, third ed. McGraw-Hill, New York.

Botwe, B.O., Abril, J.M., Schirone, A., Barsanti, M., Delbono, I., Delfanti, R., Nyarko, E., Lens, P.N.L., 2017. Settling fluxes and sediment accumulation rates by the combined use of sediment traps and sediment cores in Tema Harbour (Ghana). Sci. Total Environ. 609, 1114–1125.

Bruel, R., Sabatier, P., 2020. *serac*: a R package for ShortlivEd RAdionuclide chronology of recent sediment cores. J. Environ. Radioact. 225, 106449 https://doi.org/10.1016/j.jenvrad.2020.106449.

Caroll, J., Lerche, I., 2003. Sedimentary Processes: Quantification Using Radionuclides. Elsevier, Oxford.

Goldberg, E.D., 1963. Geochronology with Pb-210. Proceedings of a Symposium of Radioactive Dating. International Atomic Energy Agency, Vienna, pp. 121–131.

Haltia, E., Leppänen, A.-P., Kallio, A., Saarinen, T., 2021. Sediment profile dating and reconstructing nuclear events from annually laminated lake sediments in northern Finland. J. Environ. Radioact. 233, 106611 https://doi.org/10.1016/j.jenvrad.2021.106611.

Kershaw, P.J., Woodhead, D.S., Malcolm, S.J., Allington, D.J., Lovett, M.B., 1990. A sediment history of Sellafield discharges. J. Environ. Radioact. 12, 201–241.

Koide, M., Bruland, K.W., Goldberg, E.D., 1973. Th-228/Th-232 and Pb-210 geochronologies in marine and lake sediments. Geochem. Cosmochim. Acta 37 (5), 1171–1187. https://doi.org/10.1016/0016-7037(73)90054-9.

Lima, A.L., Hubeny, J.B., Reddy, C.M., King, J.W., Hughen, K.A., Eglinton, T.I., 2005. High resolution historical records from Pettaquamscutt River basin sediments: 1. [210]Pb and varve chronologies validate record of ^{137}Cs released by the Chernobyl accident. Geochem. Cosmochim. Acta 69, 1803–1812.

Mabit, L., Benmansour, M., Abril, J.M., Walling, D.E., Meusburger, K., Iurian, A.R., Bernard, C., Tarjan, S., Owens, P.N., Blake, W.H., Alewell, C., 2014. Fallout ^{210}Pb as a soil and sediment tracer in catchment sediment budget investigations: a review. Earth Sci. Rev. 138, 335–351.

Robbins, J.A., 1978. Geochemical and Geophysical applications of radioactive lead isotopes. In: Nriago, J.P. (Ed.), Biochemistry of Lead in the Environment. Elsevier, Amsterdam, pp. 285–393.

Smith, J.N., 2001. Why should we believe ^{210}Pb sediment geochronologies? J. Environ. Radioact. 55, 121–123.